

Determination of stress state in deep subsea formation by combination of hydraulic fracturing in situ test and core analysis: A case study in the IODP Expedition 319

Takatoshi Ito,¹ Akio Funato,² Weiren Lin,³ Mai-Linh Doan,⁴ David F. Boutt,⁵ Yasuyuki Kano,⁶ Hisao Ito,⁷ Demian Saffer,⁸ Lisa C. McNeill,⁹ Timothy Byrne,¹⁰ and Kyaw Thu Moe⁷

Received 26 August 2012; revised 21 December 2012; accepted 6 January 2013.

[1] In situ test of hydraulic fracturing (HF) provides the only way to observe in situ stress magnitudes directly. The maximum and minimum horizontal stresses, S_{Hmax} and S_{Hmin} , are determined from critical borehole pressures, i.e., the reopening pressure P_r and the shut-in pressure P_s , etc, observed during the test. However, there is inevitably a discrepancy between actual and measured values of the critical pressures, and this discrepancy is very significant for P_r . For effective measurement of P_r , it is necessary for the fracturing system to have a sufficiently small compliance. A diagnostic procedure to evaluate whether the compliance of the employed fracturing system is appropriate for S_{Hmax} determination from P_r was developed. Furthermore, a new method for stress measurement not restricted by the system compliance and P_r is herein proposed. In this method, the magnitudes and orientations of S_{Hmax} and S_{Hmin} are determined from (i) the cross-sectional shape of a core sample and (ii) P_s obtained by the HF test performed near the core depth. These ideas were applied for stress measurement in a central region of the Kumano fore-arc basin at a water depth of 2054 m using a 1.6 km riser hole drilled in the Integrated Ocean Drilling Program (IODP) Expedition 319. As a result, the stress decoupling through a boundary at 1285 m below seafloor was detected. The boundary separates new upper layers and old lower ones with an age gap of ~ 1.8 Ma, which is possibly the accretionary prism. The stress state in the lower layers is consistent with that observed in the outer edge of accretionary prism.

Citation: Ito, T., A. Funato, W. Lin, M.-L. Doan, D. F. Boutt, Y. Kano, H. Ito, D. Saffer, L. C. McNeill, T. Byrne, and K. T. Moe (2013), Determination of stress state in deep subsea formation by combination of hydraulic fracturing in situ test and core analysis: A case study in the IODP Expedition 319, *J. Geophys. Res. Solid Earth*, 118, doi:10.1002/jgrb.50086.

1. Introduction

[2] Motion of rocks is so slow in nature that it takes a considerable time for us to realize the motion. Contrary to this, the stress state in rocks allows us to immediately infer crustal

dynamics involving the rocks, which is typically represented as Anderson's classification of faulting, i.e., normal, thrust, and strike-slip faulting, and the stress is necessary for safe construction and maintenance of underground man-made structures, including boreholes. The first in situ stress measurement of scientific ocean drilling was carried out at Site C0009 during the Integrated Ocean Drilling Program (IODP) Expedition 319 as part of Nankai Trough Seismogenic Zone Experiment (NanTroSEIZE) Stage 2 [Saffer *et al.*, 2010; Moe *et al.*, 2012]. A new borehole, Hole C0009A, was drilled to 1603.7 mbsf (meters below seafloor) from the seafloor at a water depth of 2054 m, and hydraulic fracturing tests for stress measurement were performed using the latest wireline logging tool. A riser system used for the hole drilling made the usage of the tool possible.

[3] The hydraulic fracturing (HF) test provides the only way to observe stress magnitudes directly. In this test, a section of a borehole is isolated, and the borehole wall is subjected to increasing fluid pressure. With increasing the borehole pressure P , the hoop stress, which includes components caused by P and the maximum and minimum horizontal stresses, S_{Hmax} and S_{Hmin} , changes from compression to tension first at the two positions aligned with the azimuth

¹Institute of Fluid Science, Tohoku University, Sendai, Japan.

²OYO Co., Saitama, Japan.

³Kochi Institute for Core Sample Research, JAMSTEC, Nankoku, Japan.

⁴ISTerre, Université Joseph Fourier, Grenoble, France.

⁵Department of Geosciences, University of Massachusetts-Amherst, Amherst, Massachusetts, USA.

⁶Disaster Prevention Research Institute, Kyoto University, Uji, Japan.

⁷Center for Deep Earth Exploration (CDEX), JAMSTEC, Yokohama, Japan.

⁸Department of Geosciences, Pennsylvania State University, University Park, Pennsylvania, USA.

⁹Ocean and Earth Science, National Oceanography Centre Southampton, University of Southampton, Southampton, UK.

¹⁰Center for Integrative Geosciences, University of Connecticut, Storrs, Connecticut, USA.

Corresponding author: T. Ito, Institute of Fluid Science, Tohoku University, Sendai, Japan. (ito@ifs.tohoku.ac.jp)

of S_{Hmax} . When the combined hoop stress exceeds a tensile strength of rock, it induces tensile fractures. The fractures extend in the direction of S_{Hmax} in case of vertical boreholes such as Hole C0009A. The fractures close with venting and open with re-pressurization. In situ stress magnitudes are determined from critical borehole pressures observed during the test. The shut-in pressure P_s is used to determine the minimum horizontal stress S_{Hmin} , and the reopening pressure P_r is used to determine S_{Hmax} . The latter one is defined as the borehole pressure at the moment of fracture opening. However, a discrepancy inevitably occurs between actual and measured values of P_r due to a problem associated with the way of measurement, and sometimes it becomes very significant. For effective measurement of P_r , it is necessary for the fracturing system to have a sufficiently small compliance C [Ito *et al.*, 1999; 2005; 2006]. If not, the measured P_r becomes independent of S_{Hmax} to take the same value as P_s , in other words with S_{Hmin} . This gives a reasonable explanation for the fact that in the data of field tests so far, there is an obvious tendency for measured values of P_r and P_s to be close to each other [e.g., Evans *et al.*, 1989; Lee and Haimson, 1989; Sano *et al.*, 2005].

[4] Taking account of the effect of the system compliance C on the measurement of P_r , two strategies for determination of the in situ stresses at C0009A were applied. First, the compliance of the fracturing system composed of the dual packer tool, i.e., the Modular Dynamic Tester (MDT, Schlumberger), was evaluated, and the borehole pressure change with fracture opening upon the theoretical model considering the compliance effect was predicted. As a result, the compliance was confirmed within allowable range in which the measured P_r can be applied for determining S_{Hmax} . The S_{Hmax} and S_{Hmin} at 878.7 mbsf were accordingly determined from the measured values of P_r and P_s . Secondly, as a new idea not restricted by the system compliance and P_r , a core-based method was applied. This method assumes that a core sample retrieved from an anisotropic in situ stress field should expand elliptically in an elastic manner, the maximum expansion occurring in the direction of S_{Hmax} . The stress deviation ($S_{Hmax} - S_{Hmin}$) can be determined from the difference between the maximum and minimum diameters of the elliptical core. The S_{Hmax} can be determined as a sum of the stress deviation ($S_{Hmax} - S_{Hmin}$) and the S_{Hmin} determined from the shut-in pressure P_s , which is obtained by the in situ test of hydraulic fracturing carried out near the core depth. By this second strategy, the magnitudes of both S_{Hmax} and S_{Hmin} and the S_{Hmax} azimuth at 1532.7 mbsf were successfully determined.

2. Site C0009 and Stress State Observed in Former Expeditions

[5] The Nankai Trough Seismogenic Zone Experiment (NanTroSEIZE) is a coordinated, multiexpedition and multi-stage project of the Integrated Ocean Drilling Program (IODP). The fundamental scientific objectives of this project include characterization of the nature of fault slips and strain accumulation, fault and wall rock compositions, fault architecture, and state variables throughout the active plate boundary system. As the NanTroSEIZE Stage 1, IODP Expeditions 314, 315, and 316 were carried out in late 2007 through early 2008. These expeditions were followed

by IODP Expedition 319 as the first expedition of the NanTroSEIZE Stage 2, and two boreholes were prepared by riser and riserless drilling at Site C0009 and Site C0010, respectively. Details of this expedition have been reported by Saffer *et al.* [2010]. Site C0009 targeted in the present study is located in the central region of the Kumano fore-arc basin and the upper plate above the seismogenic and presumed locked portion of the plate boundary thrust system. A borehole, Hole C0009A, was drilled here to 1603.7 mbsf from seafloor at a water depth of 2054 m using riser drilling technology for the first time in the history of scientific ocean drilling. The upper 700 m was cased, a 12¼ inch hole was drilled from 700 to 1510 mbsf, and cores were cut from 1510 to 1539.9 mbsf using a rotary core barrel. This borehole was designed to (i) determine the composition, physical properties, and stratigraphy of the basin sediments, (ii) conduct downhole measurements to determine stress magnitude and orientation and pore pressure magnitudes, (iii) install casing in preparation for a riser observatory, and (iv) acquire data from a two-ship vertical seismic profile experiment to characterize the rock volume surrounding and below the borehole, including the subduction thrust at a depth of about 10 km.

[6] For the former stage of the NanTroSEIZE, a transect of eight sites was selected for riserless drilling to target the frontal thrust region, the midslope megasplay fault region, and the Kumano fore-arc basin (Figure 1) [Kinoshita *et al.*, 2008]. At four sites among them, i.e., C0001, C0002, C0004, and C0006 among them, borehole images were taken using the Schlumberger geoVISION LWD tool. As a result, borehole breakouts were observed at all four sites, and their orientations at three sites of C0001, C0004, and C0006 indicate northwest-southeast azimuths of S_{Hmax} . This is consistent with trench-normal shortening in the thrust dominated tectonic environment, while the S_{Hmax} orientations slightly deviate from the far-field plate motion vectors based on GPS results [Heki, 2007]. In contrast, breakouts suggest that S_{Hmax} is rotated by about 90° at Site C0002 relative to Site C0001 located at about 10 km away to the southeast. The reason for this stress rotation is still not clear but it might be caused by factors such as local deformation due to gravitation-driven extension in the fore arc and thrusting and bending within individual geologic domains. The stress analyses on breakouts in this area have been described in detail elsewhere, e.g., Chang *et al.* [2010] and Lin *et al.* [2010].

3. Hydraulic Fracturing Tests: Tool and Test Depths

[7] Borehole breakouts are well recognized as being a reliable indicator of S_{Hmax} orientation as used in the NanTroSEIZE. In this case, a breakout azimuth is applied for the stress determination. Further analyses have been made to determine even magnitude of in situ stress from breakout width along the borehole circumference [e.g., Haimson and Herrick, 1985; Brudy and Zoback, 1999; Haimson and Chang, 2002; Chang *et al.* 2010]. However, recent progress on borehole image logging indicates that there is a possibility of a significant increase in the breakout width with time [Moore *et al.*, 2011; Chang and Moore, 2012]. Such phenomena should lead to a significant error in stress magnitudes estimated from measured breakout width, while breakout azimuth is unchanged

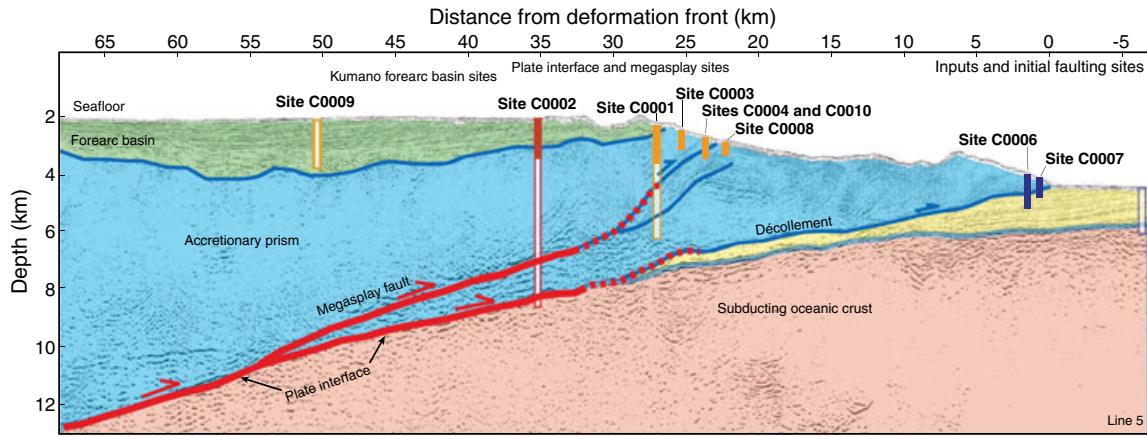


Figure 1. Drill site locations and interpreted seismic lines from *Park et al.* [2002]. Vertical lines indicate boreholes drilled at each site. Different structures are indicated with a different color, and dashed lines show megasplay fault and frontal thrust.

with time; therefore, its reliability in the determination of stress orientation remains valid. On the other hand, the hydraulic fracturing method can provide a unique measure for direct determination of in situ stress magnitude, while it requires an in situ test of hydraulic fracturing (HF) in a borehole. Thus, this method was applied for further understanding of the state of stress at Site C0009. The riser system used for drilling a hole there, Hole C0009A, made the measurement possible. The borehole tool for the HF test had a large diameter close to that of a borehole. The riser system provided easy and safe access for such a big tool to enter and exit a borehole at the seafloor far below the drill floor. *Moe et al.* [2012] reported the operational planning process related to the in situ tests carried out in Hole C0009A.

[8] The Modular Dynamic Tester (MDT, Schlumberger) wireline logging tool was used to carry out in situ tests in Hole C0009A for measurements of not only stress but also permeability and pore fluid pressure. Its modular design allows it to be customized for such multiple measurements. The configuration for Hole C0009A was set to include the gamma-ray sonde, a pump-out module (MRPO), a single probe module (MRPS), and a dual packer module (MRPA) (Figure 2). The last module is used to isolate a 1 m test interval of the borehole. The packers have a 10 inch diameter prior to inflation and are designed to plug boreholes in a range of diameters from $12\frac{1}{4}$ to $14\frac{3}{4}$ inches. The MRPO is used to pump fluid from the mud column to the packers or into the test interval. The MRPO can either withdraw or inject fluid into the test interval. Pressures in the packers and test interval are recorded simultaneously and can be displayed in real time on a monitor placed in the operator's house.

[9] In situ stress measurements by the HF test were limited to two times at different depths due to allowable cost and time. Those test intervals were selected by examining available core samples and logging data (particularly image and caliper logs). The criteria for choosing a location were (i) freedom from preexisting fractures, (ii) a hole diameter $<14\frac{3}{4}$ inches, (iii) hole ovality, i.e., maximum diameter/minimum diameter, of $<130\%$, and (iv) continuity of the above conditions for more than 3 m along the borehole. Note that the open hole section between 703.9 and 1539.9 mbsf was reamed with a $12\frac{1}{4}$ inch drilling assembly before the HF tests. Central depths of test intervals at 878.7 and

1532.7 mbsf, which were near top and bottom of the open hole section, were finally selected. The latter is located within the cored section of 1509.7–1593.9 mbsf. The HF tests and the other measurements using the MDT tool were carried out in a single run. The tool was lowered to the bottom of the hole, and the HF test was carried out, first at 1532.7 mbsf and then at 878.7 mbsf as the tool was pulled up.

4. Test Results

4.1. First HF Test at 1532.7 mbsf

[10] The standard procedure of the HF tests has been summarized by *Haimson and Cornet* [2003]. It involves a process of repeating a cycle of raising and lowering borehole pressure several times for creating (or opening) and closing hydraulically induced tensile fractures. However, the in situ conditions and the time limitation due to concerns over borehole stability did not allow us to follow this procedure. Figure 3 shows time variations of the pump-out rate, packer pressure, and borehole pressure at the test interval actually observed during the HF test at 1532.7 mbsf. The variation of borehole pressure associated with tool operation was carefully examined. The test period can be divided into three parts, i.e., periods I, II, and III. The pressure variation at each period can be interpreted as follows. For period I, pump-out fluid was supplied to inflate the packers. At time “a,” the packer pressure started to increase since the packer inflated sufficiently to fill the cross-sectional area of the borehole, and afterwards the fluid supply could contribute to elevation of the packer pressure. The packer inflated further, not in the radial direction but rather in the axial direction for a while. The axial inflation compressed fluid in the test interval, and the compression led to a pressure increase in the test interval. After termination of the fluid supply at time “b,” the interval pressure decreased not steeply but gradually. These phenomena indicate that the packers worked well to isolate the test interval and that there were no significant flow pathways such as natural fractures or breakouts to cause significant leakage from the test interval. For period II, pump-out fluid was supplied to the test interval, and accordingly, the interval pressure increased. However, the pressurization was stopped at time “c” because the pressure increase

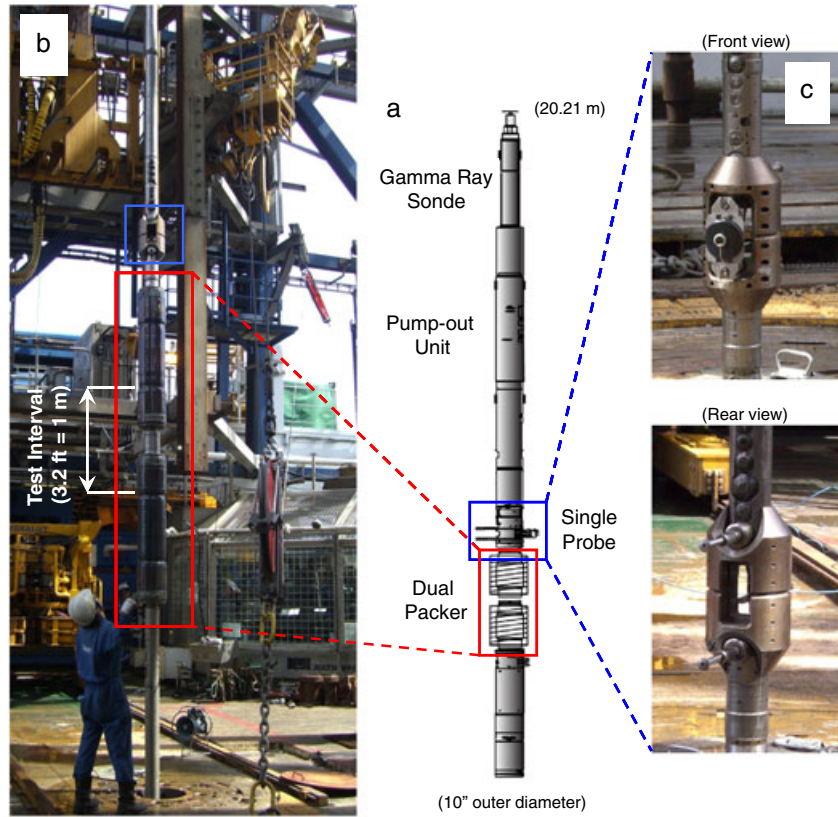


Figure 2. MDT tool employed for in situ tests at depth. (a) Overall structure, (b) dual packers and a 1 m long test interval used for hydraulic fracturing, and (c) close-up view of a single probe used for measurement of pore pressure and permeability of formations.

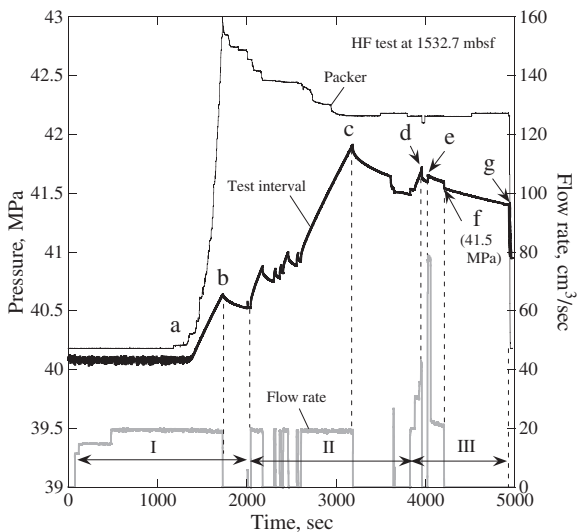


Figure 3. Variations of flow rate, packer pressure, and borehole pressure at the test interval observed during the HF test at 1532.7 mbsf.

was so gradual that it was expected to take a considerably long time until the occurrence of breakdown. For period III, the interval was pressurized again at injection rates greater than those of period II with assistance of an additional pump. As a result, the interval pressure increased more quickly to 41.7 MPa, but the pump suddenly stopped

at time “d” due to an electrical problem. After a short break for fixing the problem, the pressurization was restarted at time “e” at the maximum injection rate; however, it led to just a slight pressure increase, not reaching the pressure at time “d,” and afterwards the interval pressure decreased gradually while the fluid injection was continued at the same rate during period II. Such distinctive features which appeared in the pressure record suggest that new tensile fractures were initiated at time “d” or somewhere else between times “c” and “e.” In this case, it is most reasonable to choose the pressure at time “f,” i.e., 41.5 MPa, as the shut-in pressure P_s since P_s should appear as the point of maximum curvature on the pressure decay curve after shut-in [Hayashi and Sakurai, 1989; Hayashi and Hamson, 1991], and the pressure decay curve in the period III of the present test has the maximum curvature obviously at “f.” However, the pressure decay curve is not so typical that the detected value should be recognized to be less accurate. On the other hand, there was no way to detect the reopening pressure since this HF test was stopped at time “g” due to a time limitation related to concern over borehole stability, and the fracture reopening procedure was not applied.

4.2. Second HF Test at 878.7 mbsf

[11] Observed time variations of pump-out rate, packer pressure, and borehole pressure at the test interval are shown in Figure 4. The test period can be divided into three parts, i.e., periods I, II, and III. Period I was spent for packer inflation. Isolation of the test interval was confirmed from

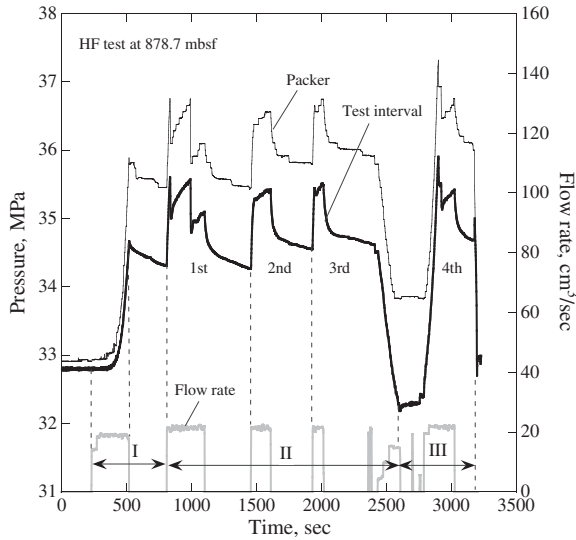


Figure 4. Variations of flow rate, packer pressure, and borehole pressure in the test interval observed during the HF test at 878.7 mbsf.

its pressure development in accordance with the packer pressurization. For period II, the pressurization of the test interval was repeated three times. The interval pressure changed typically as expected from the standard model of *Haimson and Cornet* [2003], indicating that new tensile fractures were initiated in the first cycle and reopened in the subsequent cycles. The test interval was vented to relieve excess pressure completely at the end of period II, and in period III, the last (fourth) pressurization cycle was started from a pressure slightly lower than the initial pressure in the borehole, i.e., the hydrostatic pressure. Note that venting was carried out by withdrawing the fluid in the test interval, which allowed making the interval pressure lower than the initial borehole pressure. In the fourth cycle, after the interval pressure peaked, it once decreased quickly and then increased again until shut-in, while the fluid injection was continued at a constant rate. Similar fluctuation in pressure was also observed in the first cycle. These phenomena may be interpreted as an effect of a mud cake covering the borehole wall. The borehole pressurization of the first cycle broke the mud cake, allowing fluid invasion into the induced fractures; however, it re-formed during the venting process between the third and fourth pressurization cycles. In the fourth pressurization cycle, the re-formed mud cake unexpectedly worked well to maintain the interval pressure at a level even slightly higher than the peak in the first cycle. This HF test was stopped at the end of period III.

[12] The shut-in pressure P_s and the reopening pressure P_r were obtained from the pressure-time record. To detect P_s from the pressure decay curve after shut-in, the method of *Hayashi and Hamson* [1991] was applied since the point of the maximum curvature on the pressure decay curve is hard to define directly as P_s unlike the HF test at 1532.7 mbsf. This method is based on regression analysis of the plot of dt/dP versus P , where P is pressure and t is time. Figure 5a shows the plot of dt/dP versus P obtained from the pressure decay curve after shut-in for the case of the second pressurization cycle. A straight line was fitted to the first portion of the dt/dP versus P data. The point of

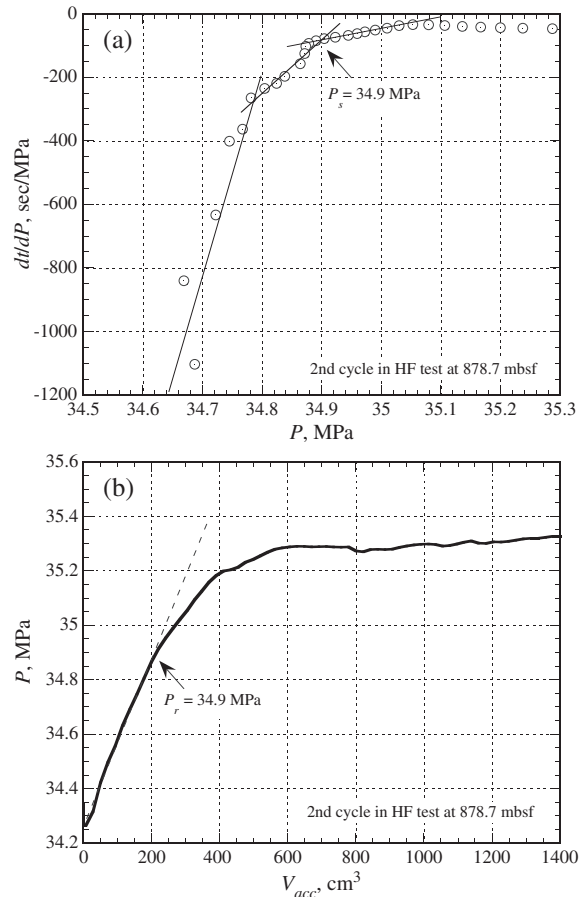


Figure 5. (a) Plot of dt/dP versus P obtained from the pressure decay curve after shut-in and (b) P - V_{acc} curve at the second pressurization cycle in the HF test at 878.7 mbsf.

departure of the remainder of the curve from the straight line was taken as P_s . As a result, P_s was determined to be 34.9 MPa. We applied the same analysis to determine P_s for the other pressurization cycles, and the results are summarized in Table 1. The reopening pressure P_r was detected from the pressure ascent curve of both the second and third cycles. This analysis was not applied to the fourth cycle since the pressure ascent curve was considered to be significantly affected by the mud cake as discussed above. Figure 5b shows the plot of P versus V_{acc} for the second cycle, where V_{acc} is the accumulated volume which was injected. The curve deviates from the initial linear trend at 34.9 MPa, so that P_r is determined to be 34.9 MPa. P_r of the third cycle was determined in the same way. The results are summarized in Table 1 together with P_s . Thus, the average P_s of four measurements is 35 MPa, exactly the same as the average P_r of two measurements, i.e., $P_s = P_r = 35$ MPa.

Table 1. Summary of Critical Pressures Detected From the Borehole Pressure and Injection Flow Rate Versus Time Record Obtained at 878.7 mbsf

Critical Pressure	Pressurization Cycle			
	Second	Third	Fourth	Average
Shut-in pressure P_s (MPa)	34.9	35.0	35.0	35.0
Reopening pressure P_r (MPa)	34.9	35.1	—	35.0

5. Stress Determination From Shut-in and Reopening Pressures

5.1. Principles

[13] When vertical fractures are induced in tension by hydraulic fracturing in a vertical borehole, the shut-in and reopening pressures, P_s and P_r , of the fractures should be related theoretically to the maximum and minimum horizontal stresses, S_{Hmax} and S_{Hmin} , as follows [Ito *et al.*, 1999]:

$$P_r = \frac{1}{2}(3S_{Hmin} - S_{Hmax}) \quad (1)$$

$$P_s = S_{Hmin} \quad (2)$$

[14] With these two equations, the values of S_{Hmax} and S_{Hmin} can be both determined from the two measured pressures of P_r and P_s . Accordingly, the measured values of $P_s = P_r = 35$ [MPa] obtained from the in situ HF test at 878.7 mbsf lead to the determined values of $S_{Hmax} = S_{Hmin} = 35$ [MPa]. The stress orientation is not a matter of course in this case. The reliability of S_{Hmin} determined from P_s by equation (2) is generally accepted. However, this is not the case for S_{Hmax} , and further examination of the in situ test conditions is required to confirm the reliability of S_{Hmax} determined from equation (1).

[15] Equation (1) includes pressure penetration into the fracture prior to fracture opening [Ito *et al.*, 1999]. As a result, the fracture begins to open at a pressure less than or equal to S_{Hmin} . The reopening pressure can be measured as a pressure at the deflection point of the borehole pressure P versus the accumulated injected volume, V_{acc} , curve. However, the effect of the initial fracture opening on the slope of $P-V_{acc}$ curve is so weak that for measurement of the actual reopening pressure given by equation (1), the compliance of fracturing system should be sufficiently small and close to the compliance of the fracture at the initial stage of fracture opening [Ito *et al.*, 1999; 2005; 2006]. The former and latter compliances refer to the system compliance C_0 and the fracture compliance C_f respectively, where C_0 is generally known as wellbore storage and C_f is defined as the increasing rate of fluid volume associated with fracture opening, V_f , driven by the borehole pressure P , i.e., $C_f = dV_f/dP$. If C_0 is fairly large compared with C_f , the measured P_r becomes independent of S_{Hmax} and has the same value as P_s , in other words with S_{Hmin} . Then the S_{Hmax} determined from equation (1) is equal to S_{Hmin} , i.e., $S_{Hmax} = S_{Hmin}$. This result is apparently consistent with that obtained from the in situ HF test at 878.7 mbsf as described above. This consistency suggests the possibility that the C_0 for the case of the HF test at 878.7 mbsf was inappropriately large for measurement of P_r . Therefore, the discrepancy between the measured and actual reopening pressures was estimated for the $P-V_{acc}$ curve simulated theoretically on conditions of the HF test at 878.7 mbsf in Hole C0009A.

5.2. Approximate Model of Borehole-Fracture System

[16] A borehole-fracture system was assumed here as shown in Figure 6, where a is the borehole radius, c is the total length of the induced tensile fracture with a residual aperture w_0 , and L is the open fracture length, i.e., the length of the section in which the aperture becomes larger than w_0 .

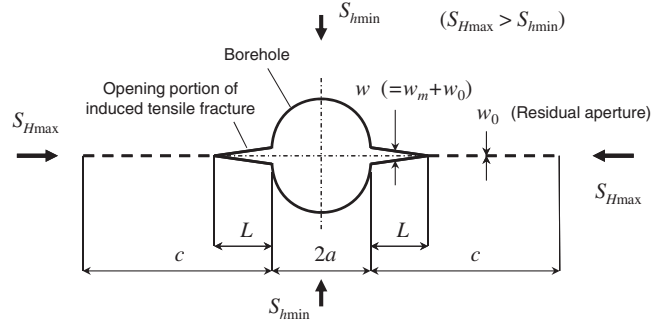


Figure 6. Illustration of the tensile fracture geometry used in the 2-D numerical simulation of fracture-opening behavior [Ito *et al.*, 1999]. The fracture aperture w is $w_0 + w_m$, where w_0 is a residual aperture persisting when the fracture is closed, and w_m is the additional opening caused by pressurization of the borehole and fracture. The length of the (additional) opened section at a given time is denoted by L .

The simulation of the $P-V_{acc}$ curve requires that a complicated problem be solved, fully coupling a compressible fluid flow and elastic deformation of a solid structure as described in detail by Ito *et al.* [1999]. However, the results of the coupled simulation show that until the borehole pressure reaches the value of S_{Hmin} , the fracture opening proceeds quasi-statically, while keeping almost uniform internal pressure balancing with the borehole pressure [Ito *et al.*, 2006]. Accordingly, if the pressure in the fracture is assumed to change uniformly with the borehole pressure, the simulation of the $P-V_{acc}$ curve becomes drastically simplified. First, the assumption allows us to determine the open fracture length L uniquely as a function of P , as follows. Fracture mechanics considerations require that the stress intensity factor K_I at the tip of the opening portion of the fracture must be zero for $L < c$. That is,

$$K_I = K_{IP} + K_{IS} = 0 \quad (3)$$

where K_{IP} is a component associated with P , and K_{IS} is that associated with S_{Hmax} and S_{Hmin} . From Tada *et al.* [1985], analytic expressions for both components are given by

$$K_{IP} = f_1(s)P\sqrt{\pi L} \quad (4)$$

$$K_{IS} = [\{f_2(s) - f_1(s)\} S_{Hmax} - f_2(s) S_{Hmin}] \sqrt{\pi L} \quad (5)$$

where $s = L/(a + L)$ and the functions $f_1(s)$ and $f_2(s)$ are given by

$$\left. \begin{aligned} f_1(s) &= 1 + (1-s) \left\{ 0.5 + 0.743(1-s)^2 \right\} \\ f_2(s) &= 0.5(3-s) \left\{ 1 + 1.243(1-s)^3 \right\} \end{aligned} \right\} \quad (6)$$

L can be determined as it satisfies equation (3) for a given value of P .

[17] Once L is known, the fracture compliance C_f can be estimated. The fracture-opening displacement $w_m (=w - w_0)$ increases the cross-sectional area of the borehole-fracture system and results in an increase in fluid volume dV_f . Areal change occurs not only in the fracture section but also in the borehole section, illustrated as a shaded portion in Figure 7a, i.e., the area of [fracture opening at the borehole wall] by [borehole diameter]. The latter plays an important role in

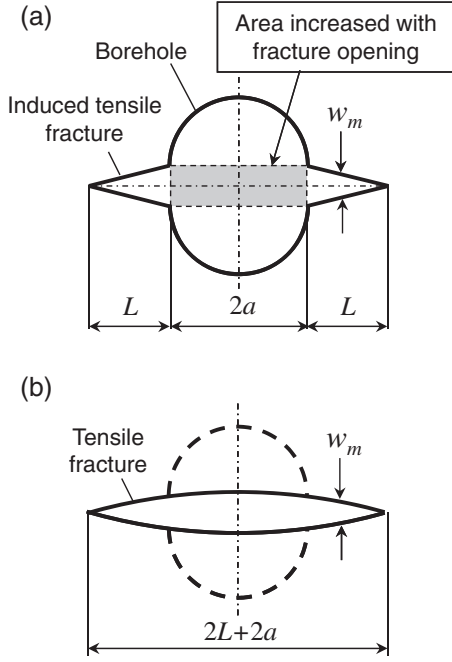


Figure 7. (a) Increase in a borehole area associated with tensile fracture opening at the borehole wall and (b) 2-D tensile fracture assumed to approximately estimate the fracture-opening displacement w_m caused by borehole pressurization.

dV_f at the initial stage of fracture opening, especially for the case of a small system compliance C_0 . In order to estimate those areal changes, the fracture-opening displacement w_m of a pressurized borehole-fracture system is here approximated by that of the uniformly pressured, 2-D bilateral fracture with length $(2L+2a)$, as illustrated in Figure 7b. Then, using the solution for a similar fracture given by Tada *et al.* [1985], the explicit expression of C_f can be deduced as follows:

$$C_f(P) \equiv \frac{dV_f}{dP} = \frac{2h(1-\nu)}{G} \left\{ (a+L)^2 \left[\frac{\pi}{2} - \frac{1}{2} \sin \left(2 \sin^{-1} \frac{a}{a+L} \right) - \sin^{-1} \frac{a}{a+L} \right] + a \sqrt{(a+L)^2 - a^2} \right\} \quad (7)$$

where h is the fracture height, ν and G are the Poisson's ratio and the shear modulus of rock, respectively. Note that (i) C_f is a function of P , since it includes L changing with P , and (ii) C_f is defined for $P > P_{r0}$, where P_{r0} is the borehole pressure given by equation (1), at which the fracture actually opens.

[18] The assumption of uniform pressure in the fracture enables further simplification of the analytical expression of the increasing rate of P with V_{acc} and results in

$$\frac{dP}{dV_{acc}} = \frac{1}{C_0 + C_f} \quad (8)$$

[19] Prior to fracture opening, C_f is zero and the borehole pressure P increases linearly with V_{acc} at a rate of $1/C_0$. This relationship is nothing but the definition of C_0 . After fracture opening, C_f becomes greater than zero, and the P - V_{acc} curve deviates from linearity. From equation (8), the relationship between P and V_{acc} is finally obtained as follows:

$$V_{acc} = C_0(P - P_0) + \int_{P_0}^P C_f dP \quad (9)$$

where P_0 is the initial value of P . Using the above equations, the P - V_{acc} curve can be easily simulated even by spreadsheet-based computation. The V_{acc} can be converted into time, t , for a constant injection rate Q by $t = V_{acc}/Q$. However, note that equation (3) is not applicable for $P > S_{Hmin}$, since it then becomes indefinite. Figure 8a shows a comparison of the above approximate simulation and the strict simulation presented in Ito *et al.* [1999] assuming, as an example, that $a = 50$ [mm], $h = 1$ [m], $G = 25$ [GPa], $\nu = 0.2$, $C_0 = 0.5$ [cm³/MPa], $S_{Hmax} = 15$ [MPa], $S_{Hmin} = 10$ [MPa], and $P_0 = 3$ [MPa]. The fracture begins to open at 7.5 MPa as estimated from equation (1). Figure 8b shows another example obtained assuming $S_{Hmax} = 20$ [MPa], while the other conditions are the same as the case of Figure 7a, where the fracture begins to open at 5.0 MPa. Both results show that the present model can simulate the P - V_{acc} curve with sufficient accuracy for detecting the apparent reopening pressure, i.e., the pressure at which the curve deviates from initial linear trend.

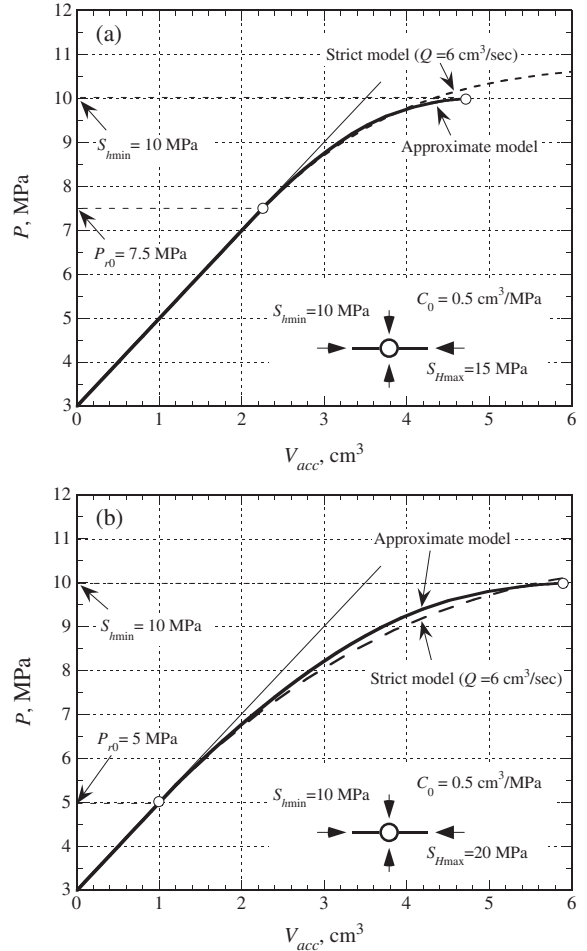


Figure 8. Comparison of P - V_{acc} curves simulated by the present approximate model and the strict model of Ito *et al.* [1999] for the cases of (a) $S_{Hmax} = 15$ and (b) 20 [MPa].

5.3. Parameter Setting and Results

[20] For simulating the P - V_{acc} curve by the present model, seven parameters, i.e., a , h , G , ν , C_0 , S_{Hmax} and S_{Hmin} , must be set in accordance with the in situ test at 878.7 mbsf in Hole C0009A, where the fracture opening is less sensitive to ν and not essentially affected by P_0 . They were set so that a is 171 mm ($6\frac{1}{8}$ in.) according to the drilling record, h is 1 m from length of the test interval, ν is 0.3 as generally assumed, and S_{Hmin} is 35 MPa from the measured shut-in pressure. Unknown S_{Hmax} is assumed here as it satisfies $S_{Hmax}/S_{Hmin} = 1.2$, i.e., $S_{Hmax} = 42$ [MPa], as an example. C_0 is determined from the in situ test data. Figure 9 shows the plot of P versus V_{acc} for the pressure ascent portion prior to the breakdown of the first pressurization cycle, in other words, prior to fracture initiation. As can be seen from equation (8), C_0 is given as the inverse of the slope of the P - V_{acc} curve because of zero C_f . The value of $C_0 = 427$ [cm^3/MPa] ($= 4.27 \times 10^{-4} \text{ m}^3/\text{MPa}$) was actually obtained from Figure 9 for use in the simulation. Finally, there remains the shear modulus G . Its value was determined from analysis combining laboratory test data by *Boutt et al.* [2012] and logging data. *Boutt et al.* [2012] conducted laboratory permeability tests on a specimen 10 cm long and 5 cm from core 4R-1 recovered at a depth of 1537.47–1537.59 mbsf as a part of cores recovered from 1509.7 to 1593.9 mbsf in Hole C0009A. The tests were carried out at a confining pressure of 10 MPa, and measurements of sample deformation during loading-unloading steps yielded a bulk modulus K of about 3 GPa. This value is converted to the shear modulus of 1.77 GPa assuming a theoretical relationship between K and G .

[21] On the other hand, G is related to shear wave velocity V_s as follows:

$$G = \rho V_s^2 \quad (10)$$

where ρ is rock density. On this relation, the shear modulus at 1537 mbsf estimated from the laboratory tests of *Boutt et al.* [2012] can be connected with the shear modulus at a depth of 878.7 mbsf as follows:

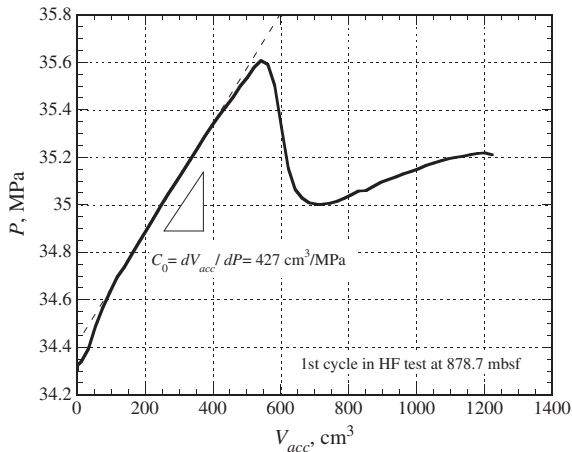


Figure 9. P - V_{acc} curve at the first pressurization cycle in the HF test at 878.7 mbsf.

$$G_8 = \left(\frac{\rho_8}{\rho_{15}} \right) \left(\frac{V_{s8}}{V_{s15}} \right)^2 G_{15} \quad (11)$$

where the subscripts of “8” and “15” are attached to each one of G , ρ , and V_s of the rocks at 878.7 and 1537 mbsf, respectively. The logging data [*Saffer et al.*, 2010] show that the rock density is almost homogeneous, being 2.1 g/cm^3 over the depth range of the open hole, i.e., $\rho_8/\rho_{15} = 1$, while the shear wave velocity at 878.7 mbsf is smaller than that at 1537 mbsf by a ratio of $V_{s8}/V_{s15} = 0.806$. Substituting these ratios and the value of G_{15} , i.e., 1.77 GPa, into equation (11), the shear modulus at 878.7 mbsf, G_8 , of 1.15 GPa is finally obtained for use in the simulation.

[22] Based on the approximate model, the relationship between P and V_{acc} was simulated for the parameter values set as above. The relationship is drawn as a curve in Figure 10a. An apparent reopening pressure of 32.3 MPa is detected on the curve, and it is slightly larger than the actual reopening pressure of 31.5 MPa estimated from equation (1). The difference is just 0.8 MPa, which corresponds to an error of less than 3%. From this result, it was concluded that the system compliance C_0 for the case of the HF test at 878.7 mbsf was within the allowable range for S_{Hmax} determination from P_r . Note that the fracture opening initiates a change in the

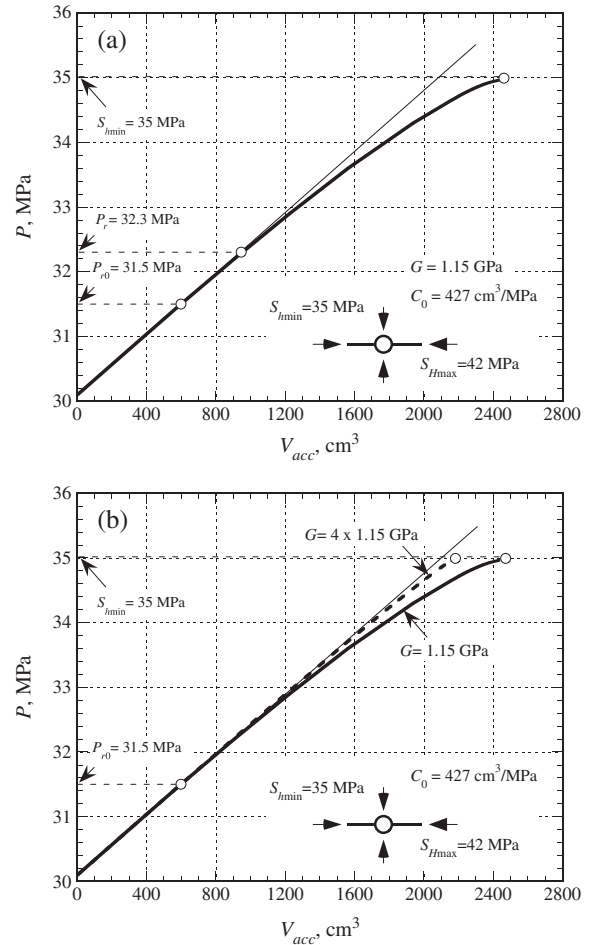


Figure 10. (a) P - V_{acc} curve at fracture reopening cycle simulated assuming the HF test at 878.7 mbsf, and (b) the curve simulated for the shear modulus which is four times as large as the case of Figure 10a.

slope of the P - V_{acc} curve more clearly for larger boreholes and softer rocks as long as C_0 does not change, since the fracture compliance C_f becomes accordingly larger as can be seen from equation (7). In the case of the HF test at 878.7 mbsf, the large borehole and the soft rock contributed well to raise C_f adequately for S_{Hmax} to be determined from P_r , even though the test system had a relatively large C_0 of $427 \text{ cm}^3/\text{MPa}$. For example, when the shear modulus G is 4 times as large as the case of Figure 10a, the P - V_{acc} relation becomes so linear, as shown by the dashed line in Figure 10b, that it becomes obviously impossible to detect P_{r0} correctly. The effect of the packer deformation constitutes a considerable ratio of the system compliance C_0 . The effect decreases with increasing inflation pressure in the packer. Thus, by setting the inflation pressure as high as possible, C_0 can be reduced even for the same setup of the test system.

6. Stress Determination From Shut-in Pressure and Core Deformation

6.1. Principles

[23] The method described in the previous section cannot be applied to the case of the HF test at 1532.7 mbsf since P_s was measured but P_r was not, which is necessary for S_{Hmax} determination. Therefore, we determined S_{Hmax} by combining with another indicator, i.e., deformation of a core sample.

[24] Let us consider the coring process. A hollow cylindrical core tube is used to obtain core samples. A core bit is pushed to the exposed surface of rock at the bottom of the borehole with a rotating motion. As a result, a column of rock is carved out and stored in the core tube. A cross-section of the carved column at the moment of drilling should be perfectly circular since the column is carved out by a rotating bit. However, a portion of the column away from the drill bit must

expand elastically in response to the relief of in situ stress. The expansion should occur in an asymmetric manner under the relief of anisotropic in situ stress field, as shown in Figure 11a. The core should expand most and least in the directions of S_{Hmax} and S_{hmin} , respectively. The stress relief induces strains in the core, which is the same as those induced in the rock mass when it is relieved from the in situ stresses, as shown in Figure 11b. If the rock is homogeneous and isotropic and is elastically deformed, the stress relief induces the tensile strains e_{max} and e_{min} in the directions of S_{Hmax} and S_{hmin} , respectively, and they are given by

$$e_{max} = \frac{1}{2(1+\nu)G} \{S_{Hmax} - \nu(S_{hmin} + S_v)\} \quad (12)$$

$$e_{min} = \frac{1}{2(1+\nu)G} \{S_{hmin} - \nu(S_{Hmax} + S_v)\} \quad (13)$$

[25] These strains can be represented by using the maximum and minimum diameter of the core, d_{max} and d_{min} , respectively, as follows:

$$e_{max} = \frac{d_{max} - d_0}{d_0}, \quad e_{min} = \frac{d_{min} - d_0}{d_0} \quad (14)$$

[26] From equations (12), (13), and (14), the differential stress in the plane perpendicular to the axis of the core can be related to the difference of diameters of the core as follows:

$$S_{Hmax} - S_{hmin} = 2G \left(\frac{d_{max} - d_{min}}{d_0} \right) \approx 2G \left(\frac{d_{max} - d_{min}}{d_{min}} \right) \quad (15)$$

While the original diameter of the core, d_0 , is unknown, the core deformation by stress relief is very minute, and d_0 in the

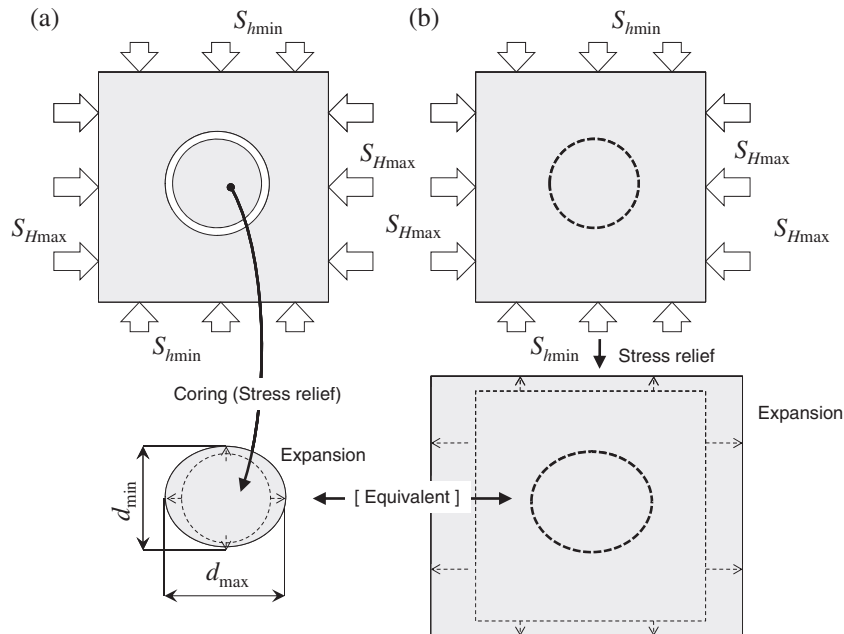


Figure 11. (a) Asymmetric core expansion resulting from coring in anisotropic stress field; (b) it is equivalent to deformation of a circular region in a rock mass due to relief of external stresses.

right side of equation (15) could be replaced by d_{\min} . Thus, the azimuths of $S_{H\max}$ and $S_{H\min}$ can be determined from the azimuths of d_{\max} and d_{\min} . This idea is advantageous in that the $S_{H\max}$ azimuth can be determined without problematic and costly measurements of the induced tensile fracture trace on the borehole wall. Furthermore, the differential stress ($S_{H\max} - S_{H\min}$) can be determined from the values of d_{\max} and d_{\min} based on equation (15). This is the basic concept of Diametrical Core Deformation Analysis, DCDA, which was originally presented by *Funato and Chen* [2005] and verified through field data analyses and laboratory experiments by *Funato et al.* [2012]. Combining DCDA with P_s or the other stress indicator of $S_{H\min}$, we can determine the magnitude of $S_{H\max}$ as a sum of the $S_{H\min}$ and the differential stress ($S_{H\max} - S_{H\min}$) from DCDA.

6.2. Diameter Measurement and Determined $S_{H\max}$

[27] DCDA requires precise measurement of core diameters in all directions. To accomplish this, the measurement tool shown in Figure 12 has been developed by *Funato and Chen* [2005]. Core diameter is measured at a resolution of $0.1 \mu\text{m}$ using an optical micrometer, while a core sample is rotated on two rollers at constant speed. The rotation rate is normally set at one rotation per 3 min, and as a result, the diameter is measured at every 2° rotation angle for the range $0-360^\circ$. As can be easily seen, one rotation, i.e., $0-360^\circ$, is redundant as it is twice the requirement for measuring circumferential diameter distribution. The additional data measured for the range $180-360^\circ$ are used for confirmation of

the measurement. Furthermore, the diameter measurements are repeated at different distances from the end of a core sample, and the consistency of those results are examined. If the deformation is not uniform along the core, the core is suspected of being disturbed by some drilling problems. The circumferential distribution of the core diameter is theoretically given by

$$d_\theta = \frac{d_{\max} + d_{\min}}{2} + \frac{d_{\max} - d_{\min}}{2} \cos 2(\alpha - \theta) \quad (16)$$

where θ is the circumferential angle measured from a reference position, d_θ is the core diameter at θ , and α is the direction of d_{\max} . This equation is fitted to the average of the observed diameter distribution by least square regression in order to find the best estimations of α , d_{\max} , and d_{\min} .

[28] We obtained core 4R-4, recovered at a depth of 1539.96–1540.16 mbsf in Hole C0009A. The diameter measurements of the core were carried out at intervals of 2 cm along the axial length between 6 cm and 12 cm from the upper end of the core sample of with a total length of 20 cm and were repeated twice at each location. The results are summarized in Figure 13, where the angle θ is measured in a clockwise fashion from a reference position defined temporarily,

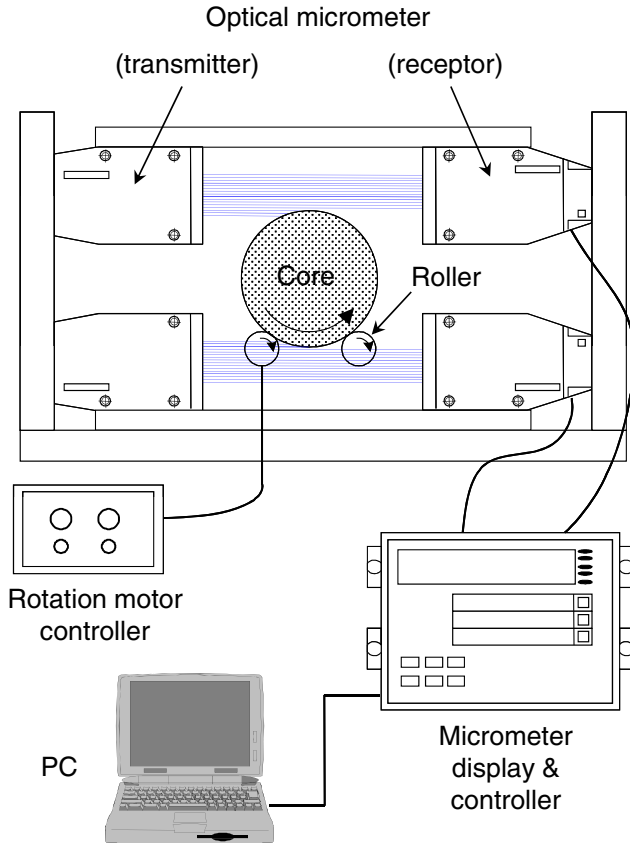


Figure 12. A system to measure circumferential variation of core diameter with resolution of $0.1 \mu\text{m}$.

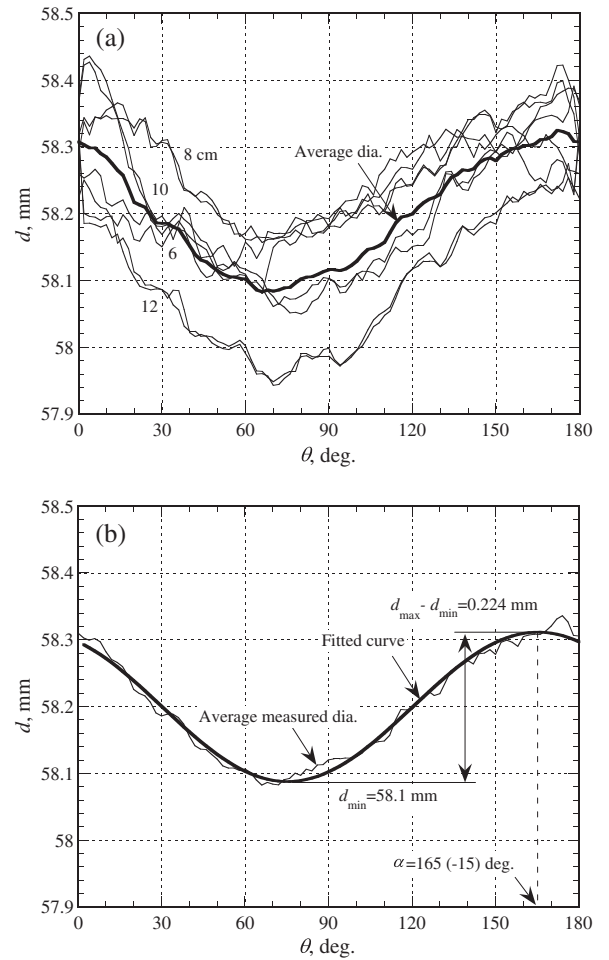


Figure 13. (a) Diameter measured at different distances, 6, 8, 10, and 12 cm, from the end of the core sample (thin lines) and their average (thick line), and (b) result of fitting equation (16) to the average by least square regression.

since the core was not oriented at drilling. The diameter measured at different distances from the end of the core sample are shown by thin lines. All of the curves are similar in sinusoidal shape. These results show that the core sample was uniformly deformed into a shape with an elliptical cross-section as theoretically expected. The thick black line represents the average of the measured diameter. By least square regression for fitting equation (16) to the average, the optimum values of $d_{\max} - d_{\min} = 0.224$ [mm], $d_{\min} = 58.1$ [mm] and $\alpha = -15^\circ$ (or 165°) were obtained. Substituting the determined diameters into equation (16), the differential stress ($S_{H\max} - S_{H\min}$) is determined to be 13.6 MPa, where for this calculation, the shear modulus of $G_{15} = 1.77$ [GPa] estimated from the laboratory tests of *Boutt et al.* [2012] was used, as described previously. Finally, we have the $S_{H\max}$ magnitude of 55.1 MPa as a sum of the differential stress and the $S_{H\min}$ of 41.5 MPa determined from P_s in the HF test.

[29] On the other hand, a borehole image log indicates a sedimentary structure with a dip of about 30° and a dip direction of $N7 \pm 12^\circ W$ at the depth of the HF test, i.e., 1532.7 mbsf [*Saffer et al.*, 2010]. An inclined sedimentary structure is also found on the surface and interior of core 4R-4, and the structure dips by about 30° in the direction of $180 \pm 5^\circ$ relative to the reference position. This structure in the core should correspond to that found on the borehole

image log. From this observation, the absolute orientation of the core can be determined by adjusting each dip direction of the core and the borehole image. As a result, the direction of the reference position is determined to be $N173 \pm 12^\circ E$, which results in the d_{\max} direction, i.e., the $S_{H\max}$ direction, of $N157 \pm 13^\circ E$ (or $N23 \pm 13^\circ W$).

[30] If P_r were to be obtained in addition to P_s by the hydraulic fracturing test, it could lead to another determination of the $S_{H\max}$ magnitude independent of the core deformation, where the system compliance should be, of course, within the range appropriate for measuring P_r , as discussed in the previous section. In this case, the $S_{H\max}$ magnitudes determined in both ways could be cross-checked. This procedure would greatly contribute to enhancement and confirmation of the determined $S_{H\max}$.

7. Summary and Discussion

[31] Figure 14a shows the magnitudes of horizontal stresses, $S_{H\max}$ and $S_{H\min}$. In this figure, hydrostatic pore pressure P_p and vertical stress S_v calculated from overburden are also plotted for comparison, where P_p was confirmed to be a hydrostatic condition by in situ tests using the single-probe module installed in MDT [*Saffer et al.*, 2010]. The $S_{H\max}$ and $S_{H\min}$ were determined assuming hydraulically induced tensile fractures with vertical orientations, as described in

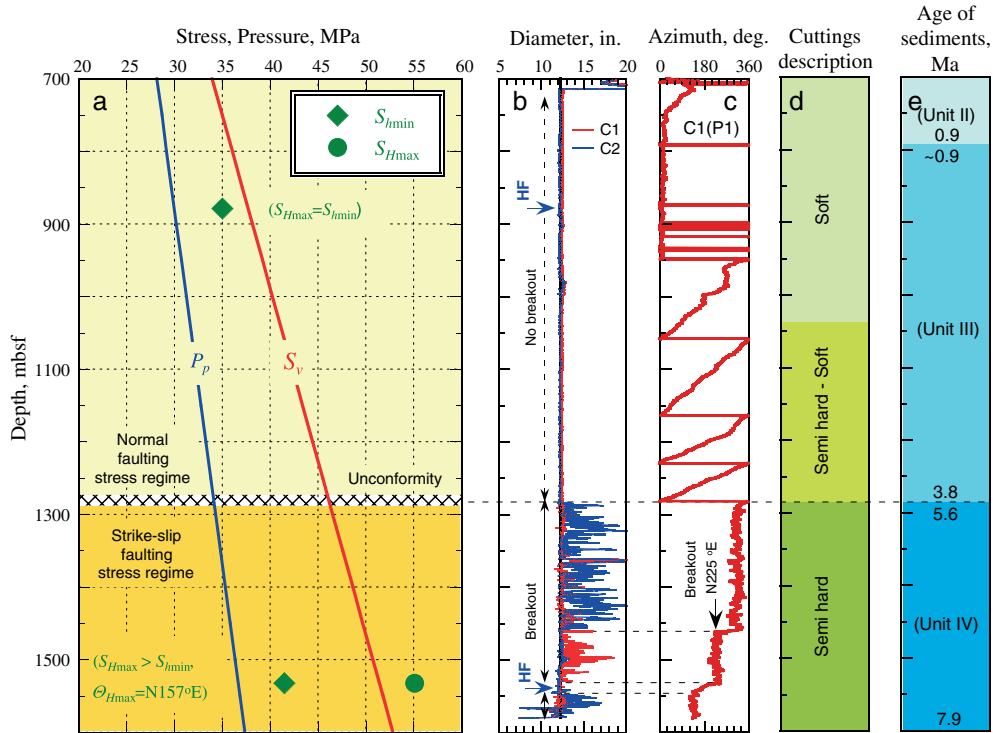


Figure 14. (a) Profile of pore pressure P_p , vertical stress S_v and the horizontal stresses $S_{H\max}$ and $S_{H\min}$ determined in the present study, where for estimation of P_p and S_v , the water density is assumed to be 1023 kg/m^3 and the rock density is assumed to be 1850 kg/m^3 for 0–703.9 mbsf and 2100 kg/m^3 for a depth deeper than 703.9 mbsf from logging data. (b) Diameters in orthogonal directions, C_1 and C_2 measured by a caliper installed in FMI, which has four arms set at every 90° , and (c) orientation of the C_1 arm, where HF shows the locations of hydraulic fracturing tests. (d) Macroscopic observation of cuttings related to hardness, where the soft and semihard designations equate to degree of consolidation and lithification, and (e) ages defined by microfossil analysis for cuttings, where the names in brackets indicate distinct lithologic units defined using the combination of data from wireline logs, cuttings, and limited core.

previous sections. Although there was unfortunately no borehole imaging logs available to identify the fracture orientation directly, this assumption is supported by the results that in both cases of 878.7 and 1532.7 mbsf, the magnitudes of S_{hmin} determined from the shut-in pressure equilibrating with the fracture-normal stress are obviously smaller than S_v . Other evidence described below was found, which verified the determined stresses as indirect proof for the assumption of fracture orientation.

[32] Several types of wireline logging runs were performed for the open hole section in Hole C0009A [Saffer et al., 2010; Lin et al., 2010]. Furthermore, the collection and analyses of drill cuttings and mud gas respectively were performed, taking advantage of the riser drilling operations applied to this hole. Many data sets obtained by those operations indicate the existence of a major boundary around 1285 mbsf. Figure 14b shows records of a caliper installed in the Formation Micro-Imager (FMI), which has four arms set at every 90° to measure borehole diameters in orthogonal directions, C_1 and C_2 . The records indicate a significant change at 1285 mbsf. Above that depth, both diameters C_1 and C_2 have the same value as the bit-size of 12¼ in. This result is harmonic with recorded orientation of the arm for C_1 (Figure 14c). The arm orientation shifts continuously with the depth of the logging tool, which should be possible because of the circular and smooth surface of the borehole. Contrary to this, below a depth of 1285 mbsf, the measured diameters indicate borehole enlargement in the direction of N225°E almost down to the bottom of the borehole, where the HF test at 1532.7 mbsf was applied to a short depth window in which the borehole remains in gauge. Such directional and continuous enlargement of the borehole is recognized as the borehole breakout resulting from a compressive failure caused by anisotropic stress concentration around the borehole. Therefore, the observed enlargement of borehole indicates the existence of considerable anisotropy in horizontal stresses, i.e., $S_{Hmax} \neq S_{hmin}$, at least below 1285 mbsf [Lin et al., 2010]. This observation is consistent with the present horizontal stresses determined by the HF test at 1532.7 mbsf and the core at 1540 mbsf, i.e., $S_{Hmax} = 55.1$ [MPa] and $S_{hmin} = 41.5$ [MPa]. In addition, the S_{Hmax} azimuth of N135 ± 11°E estimated from the breakout orientation by Lin et al. [2010] is close to that determined in the present study, i.e., N157 ± 13°E.

[33] On the other hand, the boundary at 1285 mbsf was also marked by increased lithification as shown in Figures 14d and 14e, this feature having been interpreted as resulting from secondary consolidation associated with the increased age of the sediment below the boundary by ~1.8 Ma [Saffer et al., 2010]. Thus, new soft formations above 1285 mbsf overlie old hard ones below. The difference in lithification of the new and old formations suggests that the anisotropic horizontal stresses interpreting the borehole breakout observed in the old formations should induce more severe borehole breakouts in the new formations. However, no breakouts at all were actually observed there (see Figures 14b and 14c). In order to explain such inconsistency, it is concluded that there exists stress decoupling associated with the marked change in lithology through the boundary at 1285 mbsf and that the anisotropy of horizontal stresses in the new formations at upside is much smaller than that in the old formations at downside. This conclusion is

consistent with the horizontal stresses determined from the HF test at 878.7 mbsf in the present study, i.e., $S_{Hmax} = S_{hmin} = 35$ [MPa]. At that depth, the overburden stress S_v and the pore pressure P_p are estimated to be 37.7 and 30.0 MPa, respectively. Thus, the determined state of in situ stress is categorized into the normal faulting stress regime; however, it is slightly short of the frictional equilibrium on preexisting, optimally oriented faults assuming a friction coefficient of 0.6. Such a stable stress condition may lead to sparse distribution of normal faults in the Kumano basin around Site C0009 [Saffer et al., 2010]. Note here that Lin et al. [2010] detected the drilling-induced tensile fractures (DITF) at several depths between 749 and 980 mbsf. These fractures have a nearly constant orientation at N108 ± 11 E, suggesting there was some differential horizontal stress in the interval contrary to the isotropic stress state, $S_{Hmax} = S_{hmin}$, determined in this study by the HF test at 878.7 mbsf. Considering the DITF and the fact that tensile fractures are generally sensitive to stress state, there might be actually so small difference between S_{Hmax} and S_{hmin} that the difference cannot be detected by the HF test. Accuracy of the stress magnitudes determined by the HF test depends on the detected values of P_r and P_s . For the case of the HF test at 878.7 mbsf, if there is a detecting error of ±0.1 MPa in both P_r and P_s as inferred from Figures 5a and 5b, the S_{Hmax} could be larger than the S_{hmin} by about 0.3 MPa.

[34] The S_{Hmax} azimuth has been determined so far from the borehole breakout at Sites C0001, C0002, C0004, and C0006 in this area (see Figure 1) [Chang et al., 2010]. The S_{Hmax} azimuth is oriented northeast-southwest only at Site C0002, and it is rotated by about 90° to be northwest-southeast at Sites C0001, C0004, and C0006. The latter orientation is similar to the S_{Hmax} azimuth in the formation below 1285 mbsf at Site C0009. On the other hand, the lithological analyses show that the drilled holes are fully located within the accretionary prism at Sites C0001, C0004, and C0006 and partially, i.e., below 1285 mbsf, located within it at Site C0009. Thus, the consistency in the S_{Hmax} azimuth for those four sites possibly indicates that the S_{Hmax} caused by plate motion is conveyed through the accretionary prism landward from its outer wedge. At Site C0009, such a stress state is likely decoupled from the state of isotropic horizontal stresses in the layers lying on the accretionary prism, as described above. The isotropic stress state is reasonably assumed to be formed by sedimentation in a central region of the Kumano basin where Site C0009 is located. These observations support the idea of Saffer et al. [2010] that the strange stress state at Site C0002 located at the seaward edge of the Kumano basin has been formed by some local activities such as northwest-southeast extension approximately perpendicular to the trench, which is currently in progress near the site.

8. Conclusions

[35] We presented two practical methods to measure the state of stress within a subsea formation under deep sea water. These methods are based upon findings of hydraulic fracturing tests which provide the only way to obtain the stress magnitude directly. They were applied to an offshore hole of Hole C0009A drilled using a riser system at the Kumano Basin. The hole was drilled to 1603.7 mbsf from seafloor at a water depth of 2054 m passing through an unconformity at 1285 mbsf, which possibly lies at the

boundary between the basin structure and the accretionary prism located at shallower and deeper depths, respectively. The stresses were measured at both sides, i.e., 878.7 and 1532.7 mbsf, and the results show that the maximum and minimum horizontal stresses, S_{Hmax} and S_{Hmin} , are very close at 878.7 mbsf; however, a considerable difference between them exists at 1532.7 mbsf. On the other hand, the caliper log indicates a significant change in the borehole shape at 1285 mbsf. The borehole remains in gauge down to 1285 mbsf; however, directional and continuous enlargement appears suddenly below that depth. These data suggest that the stress decoupling occurs at 1285 mbsf. While the stress state at 1532.7 mbsf is in a condition of the frictional limit for the strike-slip faulting stress regime assuming a friction coefficient of 0.6, the stress state at 878.7 mbsf is short of the frictional limit for the normal faulting stress regime. However, in both of the stress states, the least stress is near the pore pressure as expected for a subsea formation. This implies that the stress condition will be in or out of the frictional limit with a small change in the least stress or the pore pressure due to some geological events. Thus, precise stress data are important, especially for understanding subsea formation from a geophysical point of view. The methods presented in this study make it possible to obtain such precise stress data.

[36] **Acknowledgments.** The data used herein were provided by the IODP. The authors gratefully acknowledge the support provided by Expedition 319 scientists, the D/V *Chikyu* drilling crew, logging staff, and laboratory technicians. This work was supported by Grants-in-Aid for Scientific Research 21107006 (MEXT) and 24246147 (JSPS), Japan.

References

- Boutt, D., D. Saffer, M-L. Doan, W. Lin, T. Ito, Y. Kano, P. Flemings, L. McNeill, T. Byrne, N. W. Hayman et al. (2012), Scale dependence of in-situ permeability measurements in the Nankai accretionary prism: The role of fractures, *Geophys. Res. Lett.*, *39*, L07302, doi:10.1029/2012GL051216.
- Brudy, M., and M. D. Zoback (1999), Drilling-induced tensile wall-fractures: Implications for determination of in-situ stress orientation and magnitude, *Int. J. Rock Mech. Min. Sci.*, *36*, 191–215, doi:10.1016/S0148-9062(98)00182-X.
- Chang, C., and J. C. Moore (2012), Borehole breakout formation and stress estimation in unconsolidated deepwater sediments, in *Proceeding of the 46th US Rock Mechanics/Geomechanics Symposium*, Chicago, ARMA 12-447.
- Chang, C., L. McNeill, J. C. Moore, W. Lin, M. Conin, and Y. Yamada (2010), In situ stress state in the Nankai accretionary wedge estimated from borehole wall failure, *Geochem. Geophys. Geosyst.*, *11*, Q0AD04, doi:10.1029/2010GC003261.
- Evans, K. F., T. Engelder, and R.A. Plumb (1989), Appalachian stress study 1. A detailed description of in-situ stress variations in Devonian shales of the Appalachian Plateau, *J. Geophys. Res.*, *94*, 7129–54.
- Funato, A., and Q. Chen (2005), Initial stress evaluation by boring core deformation method, in *Proceedings of the 34th Symposium on Rock Mechanics, JSCE*, pp.261–266. (in Japanese)
- Funato, A., T. Ito, and T. Shono (2012), Laboratory verification of the Diametrical Core Deformation Analysis (DCDA) developed for in-situ stress measurements, in *Proceeding of the 46th US Rock Mechanics/Geomechanics Symposium*, Chicago, ARMA 12-588.
- Haimson, B. C., and C. G. Herrick (1985), In situ stress evaluation borehole breakouts-experimental studies, in *Proceedings of the 26th U. S. Symposium on Rock Mechanics*, pp. 1207–1218.
- Haimson, B., and C. Chang (2002), True triaxial strength of the KTB amphibolite under borehole wall conditions and its use to estimate the maximum horizontal in situ stress, *J. Geophys. Res.*, *107*(B10), 2257, doi:10.1029/2001JB000647.
- Haimson, B. C., and F. H. Cornet (2003), ISRM suggested methods for rock stress estimation—Part 3: Hydraulic fracturing (HF) and/or hydraulic testing of pre-existing fractures (HTPF), *Int. J. Rock Mech. Min. Sci.*, *40*, 1011–1020.
- Hayashi, K., and B. C. Hamson (1991), Characteristics of shut-in curves in hydraulic fracturing stress measurements and determination of in situ minimum compressive stress, *J. Geophys. Res.*, *96*(B11), 18,311–18,321.
- Hayashi, K., and I. Sakurai (1989), Interpretation of hydraulic fracturing shut-in curves for tectonic stress measurements, *Int. J. Rock Mech. Min. Sci. & Geomech. Abstr.*, *26*, 477–482.
- Heki, K. (2007), Secular, transient and seasonal crustal movements in Japan from a dense GPS array; implication for plate dynamics in convergent boundaries, in Dixon, T., and C. Moore (Eds.), *The Seismogenic Zone of Subduction Thrust Faults*, pp.512–539, Columbia Univ. Press, New York.
- Ito T., K. Evans, K. Kawai, and K. Hayashi (1999), Hydraulic fracture reopening pressure and the estimation of maximum horizontal stress, *Int. J. Rock Mech. Min. Sci. & Geomech. Abstr.*, *36*, 811–826.
- Ito, T., A. Igarashi, H. Ito, and O. Sano (2005), Problem for the maximum stress estimation by hydrofracturing method and its potential solution, in *Proceedings of the US Rock Mechanics Symposium*, Anchorage, ARMA/USRMS05-862.
- Ito, T., A. Igarashi, H. Ito, and O. Sano (2006), Crucial effect of system compliance on the maximum stress estimation in hydrofracturing method: Theoretical consideration and field verification, *Earth Planet and Space*, *58*, 963–971.
- Kinoshita, M., H. J. Tobin, K. T. Moe, and the Expedition 314 Scientists (2008), NanTroSEIZE Stage 1A: NanTroSEIZE LWD transect, *Integrated Ocean Drilling Program Preliminary Report, 314*, doi:10.2204/iodp.pr.314.2008.
- Lee, M. Y., and B. C. Haimson (1989), Statistical evaluation of hydraulic fracturing stress measurement parameters, *Int. J. Rock Mech. Min. Sci. & Geomech. Abstr.*, *26*, 447–456.
- Lin, W., M-L. Doan, J. C. Moore, L. McNeill, T. B. Byrne, T. Ito, et al. (2010), Present-day principal horizontal stress orientations in the Kumano forearc basin of the southwest Japan subduction zone determined from IODP NanTroSEIZE drilling Site C0009, *Geophys. Res. Lett.*, *37*, L13303, doi:10.1029/2010GL043158.2010.
- Moe, K. T., T. Ito, et al. (2012), Operational review of the first wireline in-situ stress test in scientific ocean drilling, *Scientific Drilling*, *13*, 35–39, doi:10.2204/iodp.sd.13.06.2011.
- Moore, J. C., C. Chang, L. McNeill, K. T. Moe, Y. Yamada, G. Huftile (2011), Growth of borehole breakouts with time after drilling: Implications for state of stress, NanTroSEIZE transect, SW Japan, *Geochem. Geophys. Geosyst.*, *12*(4), Q04D09, doi:10.1029/2010GC003417.
- Park, J.-O., T. Tsuru, S. Kodaira, P. R. Cummins, and Y. Kaneda (2002), Splay fault branching along the Nankai subduction zone, *Science*, *297*(5584), 1157–1160, doi:10.1126/science.1074111
- Saffer, D., L. McNeill, T. Byrne, E. Araki, S. Toczko, N. Eguchi, and K. Takahashi (2010), The Expedition 319 Scientists, Expedition 319 summary, *Proceedings of the Integrated Ocean Drilling Program*, 319, doi:10.2204/iodp.proc.319.101.
- Sano, O., H. Ito, A. Hirata, and Y. Mizuta (2005), Review of methods of measuring stress and its variations, *Bull. Earthq. Res. Inst. Univ. Tokyo*, *80*, 87–103.
- Tada H., P. Paris, and G. Irwin (1985), *The Stress Analysis of Cracks Handbook*, 2nd ed. Paris Production Inc, St. Louis, Missouri, pp. 19.1–19.3.